Final Draft
of the original manuscript:

Rao, D.; Heerens, J.; Pinheiro, G.; dos Santos, J.F.; Huber, N.:
On characterisation of local stress–strain properties in friction stir welded aluminium AA 5083 sheets using micro-tensile specimen testing and instrumented indentation technique
In: Materials Science and Engineering A (2010) Elsevier

DOI: 10.1016/j.msea.2010.04.047

On characterisation of local stress strain properties in friction stir welded aluminium AA 5083 sheets using micro-tensile specimen testing and instrumented indentation technique.

D. Rao, J. Heerens, G. Pinheiro Alves, J. dos Santos, N. Huber
Institute of Materials Research, Materials Mechanics
GKSS Research Centre Geesthacht,
Max-Planck-Straße 1
21502 Geesthacht /Germany

e-mail: juergen.heerens@gkss.de

Abstract

Stress-strain property variations in weld joints are usually characterized by determining local stress-strain curves across the weld joint. A commonly and widely accepted method is testing of micro-tensile specimens where specimens have to be mechanically subtracted form the weld-joint and subsequently tested and analysed similar to that of a conventional tensile tests. A recently developed procedure for the determination of local stress-strain properties is based on instrumented indentation testing where the force-depth curves are analysed via artificial neural networks in order to derive local stress-strain curves. In order to verify this new method for weld joints, the method has been applied to a friction stir welded 3 mm thick aluminium 5083 sheet-material. It turned out that the local-stress strain curves derived by instrumented indentation tests and neural networks are compatible with that obtained from micro-tensile specimen testing. Further on, the article gives advises on a proper tests specimen preparation as well as on the treatment of possible residual stresses. The result of this investigation support that the instrumented indentation test method combined with the application of neural networks is valid to characterise complex stress-strain property variations in friction stir weld joints.

Keywords: stress-strain properties, weld-joints, hardness, artificial neural network, residual stress

1. Introduction

Mechanical properties provide basic information on the strength of materials as for example needed for designing safe and reliable structures and components. Many properties are typically measured by uniaxial tensile tests. In cases of welded components it is often helpful to measure the Vickers hardness distribution across the weld to estimate the variation of mechanical strength and the degree of under- or overmatching [1] of the weld. Another example of application is optimisation of welding process parameters where hardness measurements are often used to monitor the associated strength variations of the weld joint [2]. Because hardness measurements provide rather qualitative information on the variation of the stress-strain behaviour, other more sophisticated methods have been developed during the last decade. One option is the determination of so called local stress-strain curves derived by testing micro-tensile specimens extracted from the weld joint [3].

Research has also focused at the capability of instrumented indentation test to provide tensile properties from spherical indentation experiments [4-7]. These tests are less destructive, quick to perform, multi-repeatable within the same weld joint and only a relatively small piece of material is required. Some of the proposed procedures are based on optimization methods coupled with elastic-plastic finite-element simulation. For power law hardening models, having only two dimensionless mechanical properties (σ_y/E, n), the inverse problem can be reduced to a unique solution given in form of a polynomial fit to an inverse function derived point wise from finite element simulations [8,9].

In cases, where more complex constitutive models are of interest, such as the unified plasticity model of Chaboche, an explicit representation of the desired inverse function determining the material parameters from measured load-depth data can not be derived such easily. Here, artificial neural networks (NN) allow analysing the available information, which is hidden in the finite element results. Huber et al. [10] applied a viscoplastic material model for simulating the indentation response of a spherical indenter. Based on that model a well-trained set of artificial neural networks for analysing the experimental force-depth curves was developed [11,12] in order to identify material property data including true stress-strain curve. Meanwhile this NN-method has become commercially available [13] and it has been successfully applied to a number of homogeneous metallic materials [14-15].

Whereas the micro-tensile specimen test technique has become common practice during the last years, little is known about the validity of the NN-method for characterising stress–strain

properties in under- or overmatched weld joints. In case of weld joints, problems may arise from the residual stresses which are usually present in the welded area. Residual stresses are affecting the force-depth curves. Because the NN-method is based on stress-free material it can not properly account for errors caused by residual stresses. Therefore, there is a high risk that a straight forward application of the NN-method to weld joints will provide invalid results.

One solution for this problem has been provided recently by a new analytical model, which allows to estimate the error in the measured hardness and to correct the force–depth curve for a known residual stress state [16]. This approach can be applied in cases where the residual stress field, i.e. the in-plane residual stress components in the indented region of the weld, is known. In most practical situations this requires additional experimental effort with X-ray or neutron diffraction and in many laboratories the experimental facilities for determining the residual stresses are not available. The goal of this paper is to provide a solution for such cases by a specific specimen preparation technique in order to enable a valid application of the NN-method.

A common way of reducing residual stresses from metal surfaces is slotting. It causes a relaxation of the residual stress present in the surface layer which is then ready for performing a valid indentation tests. Associated with such slotting it has to be taken into account that it may significantly reduce the deformation constraint of the tested volume, which biases the measured force-depth curve. In order to avoid or at least minimise such errors, clear rules regarding a proper surface cutting must be provided.

The present paper presents an example where the NN-Method is used to characterize the deformation property gradient in an under-matched friction stir weld joint by determining a set of local stress-strain curves using instrumented indentation tests. Residual stress effects were minimized by mechanical slotting of the specimen surface. Numerical simulations were performed to provide practical guidance on the slotting procedure in order to avoid an unduly high constrained reduction in the test specimen. This allows to measure force-depth curves which reflects the mechanical behaviour of the residual stress-free bulk-material.

In order to validate the local stress-strain curves derived via the indentation test method, a large set of micro-tensile specimen subtracted from the weld was also tested. It was found that instrumented indentation and micro-tensile experiments provide compatible local stress-strain curves. The results validate the specimen preparation technique as well as the indentation test approach for quantifying stress-strain property gradients in friction stir weld joints.

2. Test material, friction stir weld joint and microstructure

The material investigated was a rolled aluminium sheet-material with a thickness of 3mm of the alloy Al 5083 (Al-4.5Mg-0.6Mn). This material is widely used in ship building, tank and vehicle construction. A friction stir butt welding process was used to join the sheets. The welding was performed using a welding tool with a shoulder and pin diameter of 5 mm and 12 mm respectively. The pin rotating speed was 1800 rpm. The welding feed rate was 1000 mm/min associated with a down-load force of 9.5 kN. For more detailed information regarding the process and bonding mechanisms see [17, 18].

Figure 1 shows the macrostructure on a cross section of the weld-joint. Besides the base material (BM) it distinguishes between “advancing side” (AS) and “retreating side” (RS). Typical microstructure regions are the stir zone (Nugget), the thermo mechanical affected zone (TMAZ) and the heat affected zone (HAZ). The ring or layer structure in the centre of the figure is formed due to intensive stir which leads to bonding of the two sheets.

At higher magnification it appears that the nugget regime has very fine grains compared to that of base material (BM), HAZ and TMAZ, see Figure 2. For a more detailed description of this microstructure see [19].

An overview of the mechanical property changes across a weld can be obtained from conventional hardness measurements. Figure 3 shows the Vickers micro hardness distribution measured on the cross section of the weld joint. The BM has an average hardness about 95 HV, while the HAZ, TMAZ and nugget regime are significantly softer. The hardness profile across the weld seam seems to be asymmetrically, it decrease more sharply at the AS compared to that of the RS. Moreover, Figure 3 shows that the HAZ at the AS is smaller compared to that of the RS. Matching this hardness profile with the macrostructure in Figure 1 indicates that the HAZ of the AS is the softest zone of the weld.

3. Experimental procedures

3.1 Indentation test procedure

The indentation experiments have been performed using the Zwick testing machine ZHU0.2/Z2.5, which is equipped with the hardness measuring head and fully automated X/Y

table [20]. . The built-in load cell measures electromechanically applied forces between 2 N and 200 N with the force resolution of 0.01 N and displacement measuring resolution of 0.02 µm. Integrated in the hardness measurement head are a digital travel measurement system on a glass scale with a resolution of 0.04 µm, a load cell and an interchangeable indenter. A diamond Rockwell indenter with a spherical tip radius of 200 µm was installed and used for all tests. In the data analysis the residual stiffness of the testing equipment was set to be C = 2.5 x10^5 mN/µm. All experiments were performed in an air-conditioned room at a temperature of 21°C using load-control mode.

The indentation tests were performed with the multi-creep loading history consisting of three creep segments at 0.25 P_0, 0.5 P_0 and 0.75 P_0 of 100s duration and a final creep segment at maximum load P_0 of T_4 = 600 s [21]. Another additional reloading-unloading process with 1.25P_0 of 2s duration is executed to complete the hysteresis loop of the 4th cycle. The maximum load P_0 has to be set to achieve the indentation depth h_0 in the range of 8% to 12% of the nominal indenter radius of 200 µm. For the alloy investigated, the maximum load, P_o, was set to 20 N with the load application rate in overall experiment 0.5 N/s. A schematic of the loading history is shown in Figure 4.

Neural Network Analysis Method

This method for analysing indentation curves via neural networks of the “ASMEC Indenter Analyser” [13] is based on a viscoplasticity model, which decomposes the total stress into a rate independent equilibrium stress $\sigma^{(E)}$ and the rate dependent overstress F. Their sum is the total stress for a given plastic strain and plastic strain rate. For small deformation theory and monotonic tensile loading the model can be simply written as [11]:

$$\sigma(\varepsilon_p, \dot{\varepsilon}_p) = \sigma^E(\varepsilon_p) + F(\dot{\varepsilon}_p) = k_0 + \frac{\gamma}{\beta}(1 - e^{\beta\varepsilon_p}) + \frac{3}{2}\frac{c}{b}(1 - e^{b\varepsilon_p}) + (\eta\dot{\varepsilon}_p)^{1/m} \qquad (1)$$

As written in (1), the equilibrium stress can be decomposed into its contributions, which are the isotropic and the kinematic hardening, each determined by two material parameters γ, β , and c, b, respectively. The yield stress, k_0, is given by the value of the isotropic hardening at zero plastic strain. When we assume that the hardening is purely isotropic, data from unloading-reloading hysteresis are ignored and (1) is reduced to

$$\sigma(\varepsilon_p, \dot{\varepsilon}_p) = k_0 + \frac{\gamma}{\beta}(1 - e^{\beta\varepsilon_p}) + (\eta\dot{\varepsilon}_p)^{1/m}. \qquad (2)$$

The viscosity exponent *m* and the viscosity parameter η define the rate- dependent amount of overstress *F*. The maximum equilibrium stress is given by $\sum = k_0 + \gamma/\beta$, where the fraction γ/β defines the maximum amount of work hardening during plastic deformation.

Using a set of well trained artificial neural networks, described in detail in [11,12] the material parameters in (1) or (2) and consequently the stress-strain behaviour of a material can be identified. Meanwhile, this neural network software is commercially available [13].

Indentation specimen preparation

A successful determination of local stress-strain curves via the NN-Method requires a high quality experimental determination of the force-depth curves. Frequently observed errors are associated with the preparation of the test specimen [22]. In cases where a standardized Rockwell indenter with a tip radius of 200 μm is used for the indentation tests, the maximum indentation depth at the end of the tests has to be within the range from 15 μm to 25 μm. This means that roughness of the indentation surface or possible cold work material hardening in the surface layer due to milling, drilling or other mechanical treatments can significantly affect and spoil the force-depth curve. An often observed error source is unexpected test specimen movement due to an insufficient fixing of the specimen during the indentation test. Therefore, associated with the preparation of test specimen the user has to be aware of several factors which can bias the measured force and depth data.

To enable high quality indentation tests, rectangular sections have been extracted from the welded seam. The sections were then imbedded into thermosetting synthetic resin. The top and bottom side of the resin block were then milled and grained to provide even surfaces. Finally the top side (indentation-surface) of the block was mechanically polished with abrasive paper from 80-grade down to 2400-grade following by diamond polishing with abrasive grit size of 3 μm and finalized with polishing SiO_2-solution. After this procedure the specimen surface on the top side of the block showed mirror quality associated with a surface roughness of R_a=0.2 μm.

In order to avoid an influence of the in-plane residual stresses, the top surface of the imbedded test specimen was slotted. It produced a well defined pattern of slots with 3 mm in distance and depth, see Figure 5.

Micro tensile tests

Micro-tensile specimens have been machined by electrical discharging. This was done by sectioning the base material and the weld joint into thin slices as illustrated in Figure 6. About 50 micro-tensile specimens were machined, which sample the BM, HAZ, TMAZ and the nugget across the entire weld joint from the AS to the RS. The thickness of the specimen was about 0.4 mm. The specimen width in the mid section and grip regime was 1.4 mm and 2.5 mm, respectively. During the tensile test the elongation of the specimen was measured within the mid section of the specimen via an initial gauge length, l_0, of 8 mm by using a laser extensometer (Fiedler P50). A special specimen fixture was used to assure uniaxial and bending-free loading condition of the micro-tensile specimens.

4. Results and Discussion

Influence of specimen surface slotting on force-depth curves

To assure a relaxation of possible residual stresses within the indentation test specimen, a series of fine slots was machined into the test specimen surface using a fine diamond saw blade. It produced an array of small cubes of material as displayed in Figure 5. In order to verify how this slotting is affecting the force-depth curve due to a change of constraint, the slotted geometry has been modelled using an axisymmetric finite element model with variable slot distance and depth, see Figure 7. The simplification from slotted cube with a side length $2L$ to a column with a diameter and depth of *2L* is conservative with regard to a possible constraint on the indentation force and unloading stiffness. A rigid contact surface was used to model the spherical indenter, which is displaced by maximum h=0.1R into the specimen surface.

A stress-strain curve derived by conventional tensile tests on base material has been used as input for the calculations in form of a multi-linear plastic strain-stress relation. All nodes on planes x=0, and y=0 are fixed in these respective directions to model the symmetry conditions. The simulations are performed using ABAQUS. Simulations have been performed for different column radii, L. To simulate 6 different column sizes, the Young's modulus of the selected slot elements, displayed by the lines in Fig. 7, have been set to a very small value of 1 GPa.

As a summary of the simulations, Figure 8 displays the influence of the column size to indenter radius ratio, L/R, on both the indentation force, F, and the unloading stiffness, S, at a fixed indentation depth of 0.1R. The curves F/F_0 and S/S_0 represent the percentages of remaining force and unloading stiffness of the slotted specimen with respect to the non-slotted specimen. With increasing L/R, the influence of the free boundary on the indentation force F and unloading stiffness S diminishes gradually. As a first approximation we can assume that the effect decreases exponentially with increasing slot distance L/R. By fitting the finite element results we obtain fit functions of the form $F/F_0 = 1 - 0.094\exp(-0.45L/R)$ and $S/S_0 = 1 - 0.237\exp(-0.25L/R)$ for the force and unloading stiffness reduction, respectively.

In our indentation tests the slot distance and indenter tip radius are 2L=3 mm and R=0.2 mm which yields an L/R-ration of 7.5. For such test condition the slots are affecting the indentation force and unloading stiffness by less than 0.5% and 4%, respectively, see Figure 8. For most engineering applications this small effect is negligible. Hence, it can be assumed that the force-depth curves measured under such condition is reflecting the mechanical property of non-slotted bulk material.

Local stress-strain curves across the weld seam.

The diagrams in Figures 9 to 11 show local stress-strain curves as derived from micro-tensile specimens and indentation tests applied to a non-slotted (as-welded) and slotted indentation specimen. Each Figure presents two sets of local stress-strain curves derived along a 40 mm long path across the weld joint. One set shows the stress-strain property of base material. The second set represents the stress-strain property of material within the weld region which tends to be softer than the base material. The stress-strain property gradient is also displayed in Figure 12a,b. It shows true stress-values across the weld seam associated with two distinct true strain-values of 4% and 8% as obtained form the stress-strain curves in Figure 9 to 11. The vertical dotted lines in Figure 12 indicate the position where the border between base material and weld material region was defined.

Due to a relatively fine sectioning across the weld, 46 local stress-strain curves have been determined across the weld seam using micro-tensile specimens. Indentation test on as-welded specimen with a distance of 1 mm between the individual indentation points resulted in 32 stress-strain curves. In case of the slotted specimen, single indentation tests were

performed at the centre of each small square visible at the specimen surface in Figure 5. It yielded 12 stress-strain curves in total.

True stress-strain data as obtained from micro-tensile tests were calculated by converting the engineering stress and engineering strain data by the following Equations:

$$\sigma_{true} = \sigma_{eng}\left(1+\varepsilon_{eng}\right); \quad \varepsilon_{true} = \ln\left(1+\varepsilon_{eng}\right); \qquad (3)$$

The application of Equation (3) becomes invalid in the regime where the micro-tensile specimen starts to show local necking. Therefore, the ends of individual stress-strain curves displayed in Figure 9b coincide with a start of specimen-necking rather than with final fracture of the tensile specimens. In general it was observed that necking of base material specimen starts at much smaller strains compared to that of weld material. For this reason the number of base material stress-strain curves becomes drastically reduced at strains larger than 8%. In contrast to micro-tensile test method, the nature of indentation tests excludes specimen-necking and specimen-fracture. Therefore, any indentation test provides a true stress-strain curve, which is available over the entire strain regime displayed in Figure 10 and 11.

Many investigations have indicated that local stress-strain curves derived by micro-tensile specimen testing are very useful input quantities for numerical calculations aimed at the prediction of the mechanical behaviour of weld joints and welded structures. Examples are given in [23,24]. To introduce indentation testing as a more efficient technique, it is of interest to compare the stress-strain curves obtained by indentation test with that of micro-tensile specimen testing. Comparing the stress-strain curves in Figures 9 to 11 by eyeball it is obvious that the indentation tests on as-welded and slotted specimens provide stress-strain curves which are similar to that of micro-tensile testing. Because the numbers of stress strain-curves, (N), in Figure 9 to 11 are different, a more meaningful interpretation of the curves is obtained by considering average-value stress-strain curves and the corresponding standard deviations. Figures 13a and b display average-value curves of the weld region material and base material as calculated form the individual curve set shown in Figures 9 to 11. In case of weld region material excellent agreement between the average-value curves obtained from micro-tensile tests and indentation tests on slotted specimens is observed. In contrast to the slotted specimen, the average-value curve obtained form as-welded specimens provide about 10 % higher stresses. Figure 13b considers average-value curves as derived from base material. It appears that the curves obtained form micro-tensile tests in

tend to show a larger curvature than the curves obtained form indentation tests, which is the main reason for curve differences in Figure 13b. The effect is most pronounced for the as-welded specimen and leads to a significant stress overestimation with increasing strains. The curves in Figure 13a and b demonstrate that such stress overestimation can be avoided by using slotted indentation tests specimens.

Micro-tensile specimen testing and indentation testing also provide an estimate of the Young's Modulus, *E*, and the 0.2% offset yield strength, $R_{p0.2}$, see 14a,b. Figure 14a displays a representative selection of local stress-strain curves of base material obtained form micro-tensile tests. The elastic slopes of the curves reveal Young's Moduli which are within the range from 63 GPa to 78 GPa. The indentation tests on slotted specimens provides E-values of about 70 GPa (see Figure 14b) which fits well to that observed for micro-tensile specimens. In case of as-welded specimen the indentation tests provide Young's Moduli of the order of 80 GPa which tends to be unrealistically large for this Al-alloy.

Considering the $R_{p0.2}$-values in Figure 14 it can be seen that the $R_{p0.2}$-values of the indentation tests show much larger scatter compared to that of micro-tensile tests. This behaviour is typical for non-homogeneous materials because the indentation test is reflecting a material property average which is associated with a much smaller test volume compared to that of the micro-tensile specimen. Nevertheless, the average of the R_{p02}–values obtained from indentation tests on slotted, as-welded and micro-tensile are not significantly different.

In summary, the investigations show that indentation tests combined with the NN-method is able to provide local stress-strain curves which characterise the stress-strain property variation across a FSW-weld joint of AA 5083 sheet material. The derived local stress-strain curves, Young's Modulus and $R_{po.2}$–values are consistent with that obtained from flat micro-tensile specimens. The agreement between the results of different methods can be improved by a proper slotting of the indentation test-specimen which assures a relaxation of residual stress without an inadequate large relaxation of plastic constraint within the indentation surface. As quantified by finite element simulations the slotting pattern as used in this investigation reduces the indentation force and unloading stiffness by less than 0.5% and 4%, respectively, which is considered as negligible in engineering applications.

The promising results of this investigation demonstrate that instrumented indentation method combined with NN-method is valid for characterising weld joints. In addition, the advantages of an easy and fast application of the method as well as the small required tests volumes offer a number of interesting applications for example in the fields of weld joint

characterization, weld process optimization, quality assurance or structural assessment, that are aspects presently under investigation at GKSS.

5. Summary

This article shows that local stress-strain curves obtained from the indentation tests and neural networks analysis are in very good agreement with that obtained from the conventionally used micro-tensile tests method. This demonstrates the validity of the instrumented indentation test method to provide local stress-strain curves with less experimental effort. It has been shown that this is an efficient approach for determining the complex stress-strain property variations in friction stir welded Al 5083 sheet material.

Particular good agreement between the local stress-strain curves as derived by the two different tests methods have been obtained in cases where the surface of the indentation specimen has been slotted in order to reduce possible residual welding stresses present in the surface layer of the test specimen.

Based on finite element simulations, this article also provides guidance on the proper slotting geometry of the specimen surface in order to ensure valid local stress-strain curves which are reflecting the mechanical behaviour of bulk-material.

The advantages of an easy and fast application of the indentation test method as well as the small required tests volumes offer a number of interesting applications in the field of mechanical weld joint characterisation. Other types of weld joints and metallic materials are presently under investigation in order to gain a broader knowledge about the applicability and validity of this indentation test method.

6. References

[1] A. Motarjemi, M. Kocak, V. Ventzke, Mechanical and fracture characterization of a bi-material steel plate, International Journal of Pressure Vessel and Piping, **79**, 181-191 (2002)

[2] S.T. Amancio, S. Sheikhi, J.F. dos Santos, C. Bolfarini, *Preliminary study of the microstructure and mechanical properties of dissimilar friction stir welds in aircraft aluminium 2024-T351 and 6056-T4*, Journal of Materials technology, in press (2008)

[3] Ü. Ceyhan, *High Temperature Deformation an Fracture Assessment of Similar Steel Welds*, Clausthal-Zellerfeld: Papierflieger, (2007) ISBN: 978-3-89720-882-7*Pb http://www.gbv.de/dms/clausthal/E_DISS/2007/db108543.pdf,

[4] J.S. Field and M.V. Swain, *Determining the mechanical properties of small volumes of material from sub micro indenter spherical indentations*, J. Mater. Res.,**10**, 101-112 (1995).

[5] B. Taljat, T. Zacharia, *New analytical procedure to determine stress-strain curve from spherical indentation data*, Int. J. Solids Structures, **35** (33); 4411-4426 (1998).

[6] S. Kucharski, Z. Mroz, *Identification of plastic hardening parameters of metals from spherical indentation tests*. Materials Science & Engineering 318 (1-2):65–76 (2001).

[7] S. Kucharski, Z. Mroz, *Identification of hardening parameters of metals from spherical indentation test.* Journal of Engineering Materials and Technology-Transactions of the ASME 123; 245–250 (2004).

[8] M. Zhao, N. Ogasawara, N. Chiba and X. Chen, *A new approach to measure –elastic-plastic properties of bluk materials using spherical indentation*, Acta Materialia, **54**, 23-32 (2006).

[9] Y. Cao, X. Qian, N. Huber, Spherical indentation into elastoplastic materials: Indentation-response based definitions of representative strain, Materials Science and Engineering A 454-455, 1-13 (2007)

[10] N. Huber and Ch. Tsakmakis, *A new loading history for identification of viscoplastic properties by spherical indentation*, J. Mater. Res. **19** (1); 101-113 (2004).

[11] E. Tyulyukovskiy, N. Huber, *Identification of viscoplastic material parameters from spherical indentation data: Part I. Neural networks*, J. Mater. Res., **21** (3); 664-676 (2006).

[12] D. Klötzer, Ch. Ullner, E. Tyulyukovskiy, N. Huber, *Identification of viscoplastic material parameters from spherical indentation data: Part II. Experimental validation of the method*, J. Mater. Res., **21** (3); 677-684 (2006).

[13] ASMEC Advanced Surface Mechanics GmbH, Radeberg, Rossendorf Germany; http: //www.asmec.de/software/IndentAnalyser-Help.pdf

[14] E.Tyulyukovskiy N.Huber, *Neural networks for tip correction of sperical indentation curves from bulk metals and thin films*, Journal of Mechanics and Physics of Solids, **55**, 391-418 (2007).

[15] N. Huber, E. Tyulyukovskiy, H.-C. Schneider, R. Rolli, M. Weick, *An indentation system for determination of viscoplastic stress-strain behaviour of small metal volumes before and after irradiation*, Journal of Nuclear Materials, **377**, 352-358 (2008)

[16] N. Huber, J. Heerens; On the effect of general residual stress state on indentation and hardness testing, Acta Matarialia, **56**, 6205-6213 (2008)

[17] H.N.B.Schmidt, T.L.Dickerson, J.H.Hattel, *Material flow in butt friction stir welds in AA 2024 T3* Acta Materials, **54**, 1199–1209 (2006)

[18] K.N.Krishnan, *On the deformation of onion rings in friction stir welds*, Materials Science Engineering A **327**, 246–251 (2002)

[19] D. Rao, J. Heerens, G. Pinheiro Alves, J. dos Santos; *The Microstructure and mechanical property asymmetry of ally 5083 friction stir welding joint*, in preparation

[20] *Testing Machines and Systems for Metals (brochure*); available at: http://www.zwick.com/frame/Control.php?action=Frame,show&mainNavId=11,

[21] E. Tyulyukovskiy, *Indentification of mechanical properties of metallic materials from indentation tests,* Ph.D. Thesis, FZKA-Report 7103, March (2005), <http://bibliothek.fzk.de/zb/berichte/FZKA7103.pdf

[22] J. Heerens, F. Mubarok an N. Huber; *Influence of specimen preparation, microstructure anisotropy, and residual stresses on stress-strain curves of rolled Al2024 T351 as derived from spherical indentation tests*, J. Mater. Res., **24** (3) 907-917 (2009)

[22] I. Scheider, Brocks W. and A. Cornec; *Procedure for the determination of true stress-strain curves from tensile tests with rectangular cross- section specimen*, Trans. ASME, J. Eng. Mater. Tech. **126** (2004)

[23] P. Cambresy *, Damage and fracture mechanism investigations of an aluminium laser beam weld*, Report of GKSS Research Centre, GKSS 2006/5 (2006)

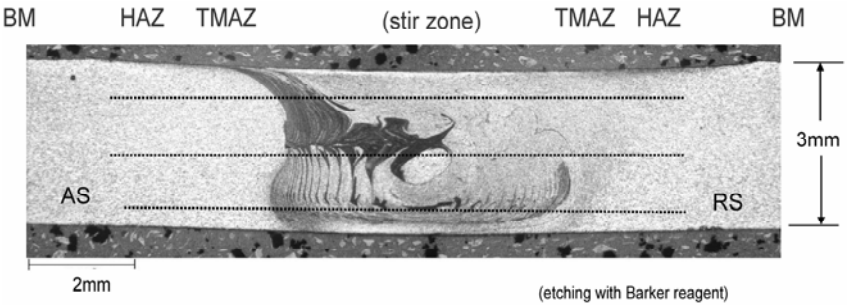

Figure 1:

Macrostructure of the 5083 FSW-joint.
The dotted up-, middle- and bottom-lines indicate paths of hardness measurements.

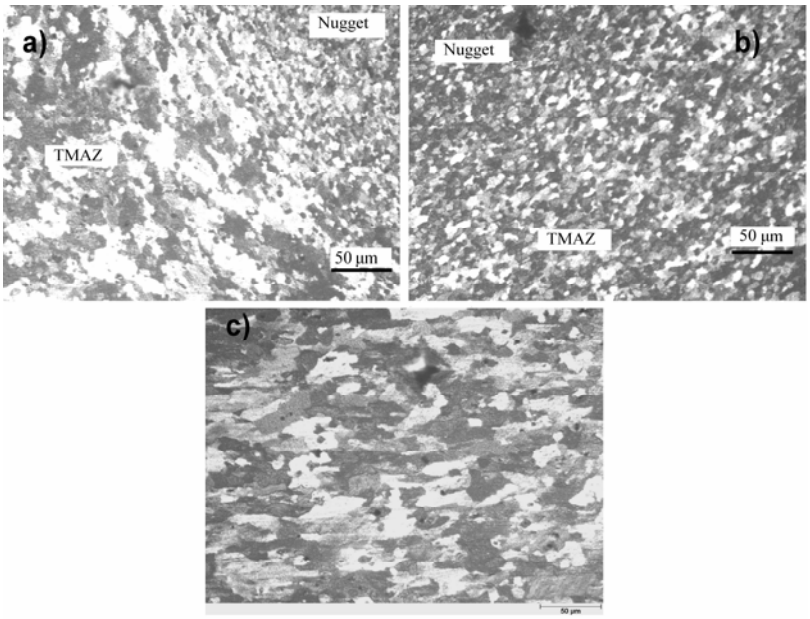

Figure 2:

Typical microstructure of the FSW-joint:
a) TMAZ/Nugget on AS
b) TMCP/Nugget on RS
c) BM (base material)

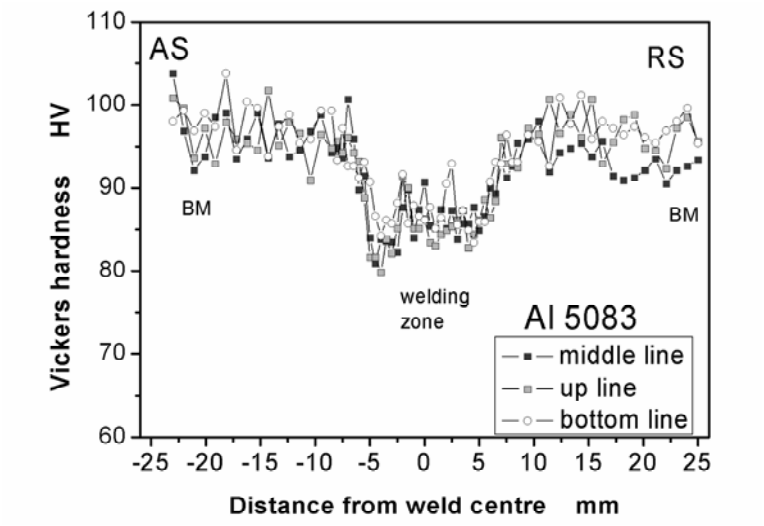

Figure 3:
Hardness measured at three paths across the FSW weld seam, seen in Fig.1.

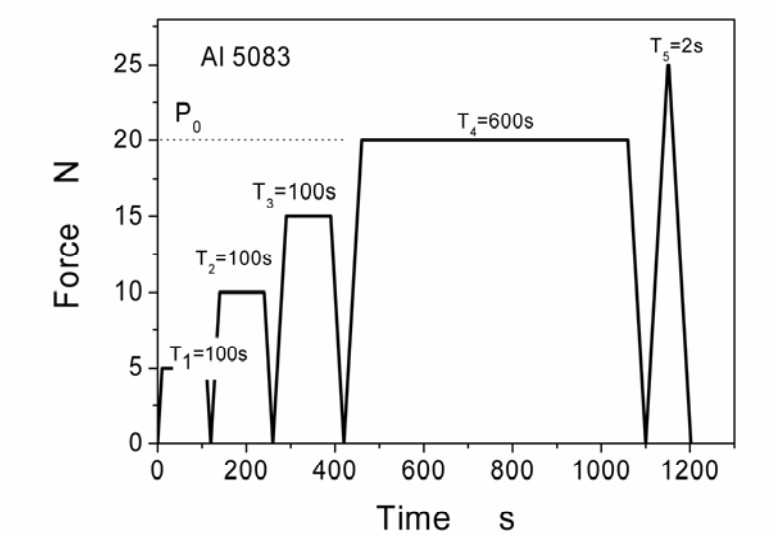

Figure 4:
Force-time-function as used for the indentation tests.

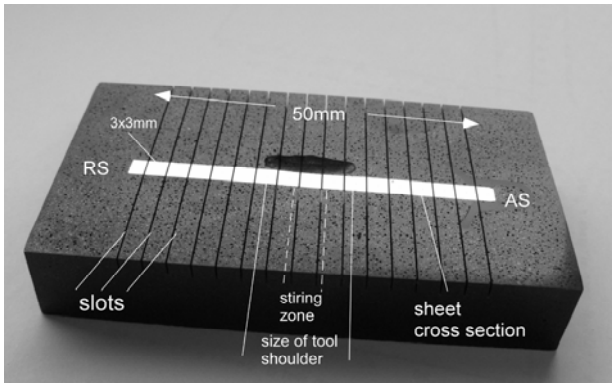

Figure 5:

Indentation test specimen imbedded in synthetic resin. The indentation surface was slotted in order to reduce the in-plane residual stresses.

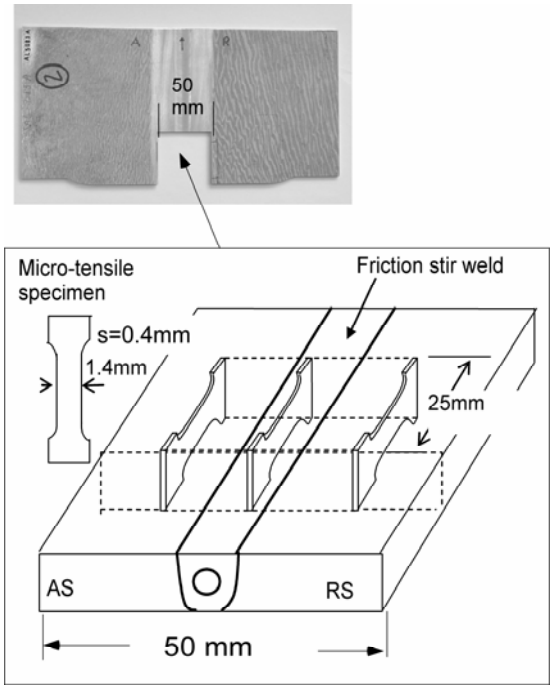

Figure 6:

Micro-tensile specimens machined from the FSW-weld joint by electrical discharging technique.

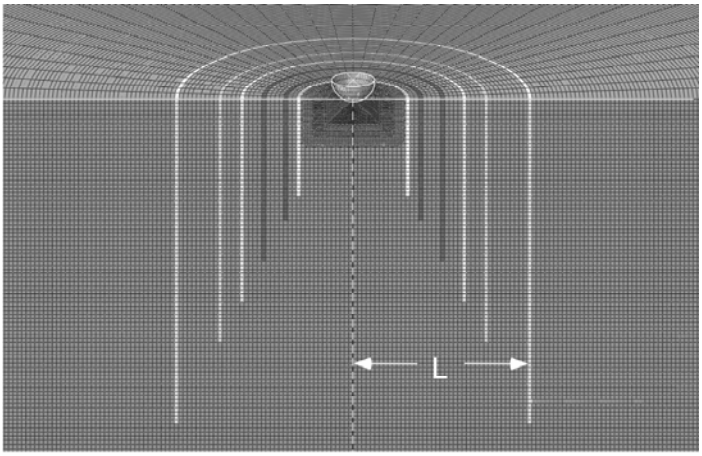

Figure 7:

2D finite element mesh visualised as swept model. The individual lines are slots which form 6 columns (volumes) of different size with a radius of L and depths of $2L$.

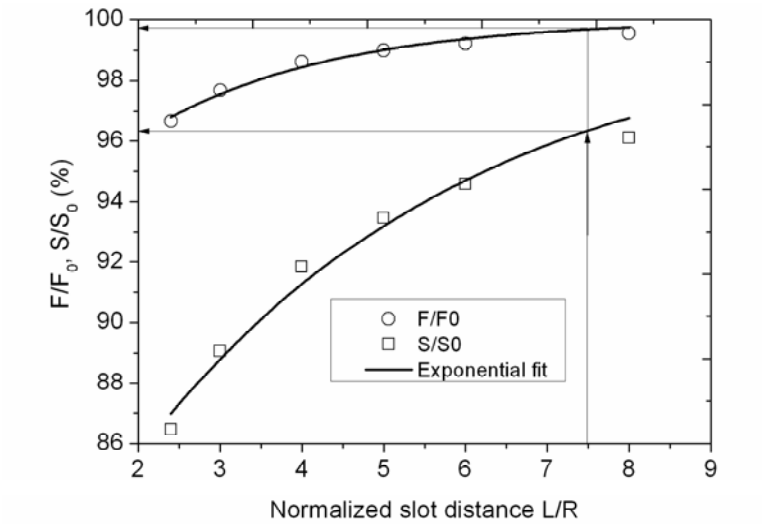

Figure 8:

Influence of column volume on indentation force, F, and unloading stiffness, S, at fixed indentation depth of h/R = 0.1. Arrows are marking the tests condition of the slotted test specimen shown in Figure 5.

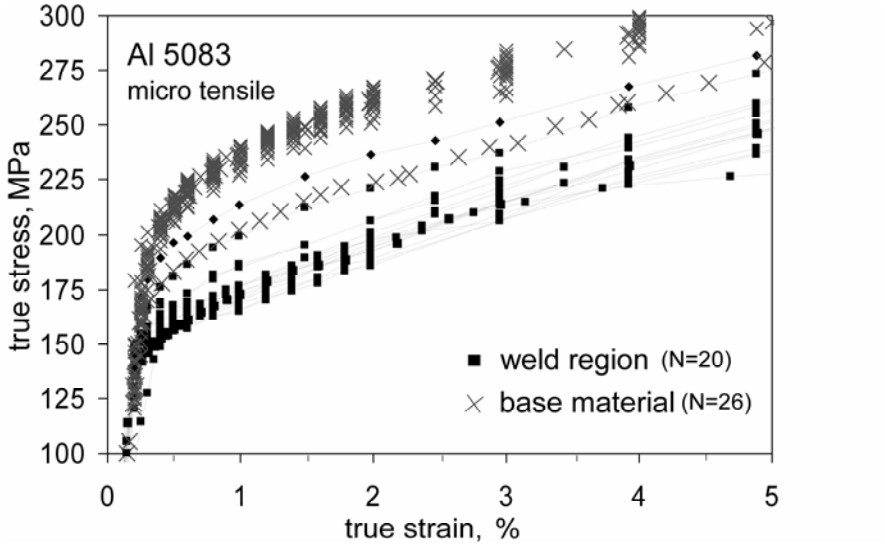

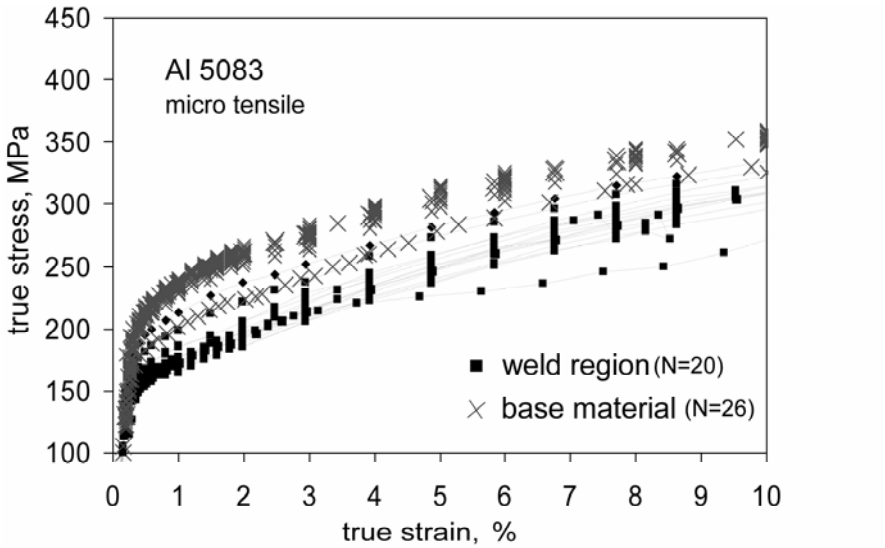

Figure 9a,b:

Local stress-strain curves across the FSW-joint obtained from micro-tensile specimen tests; a) and b) show same curves at different scale.

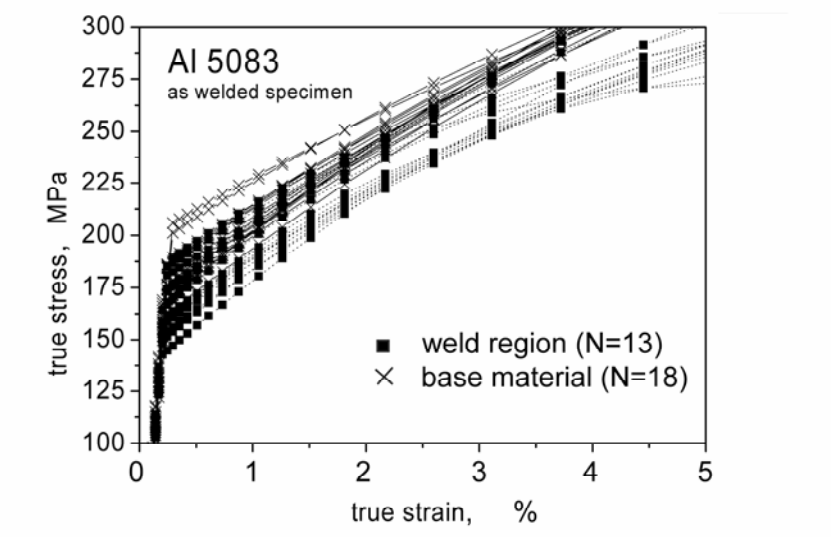

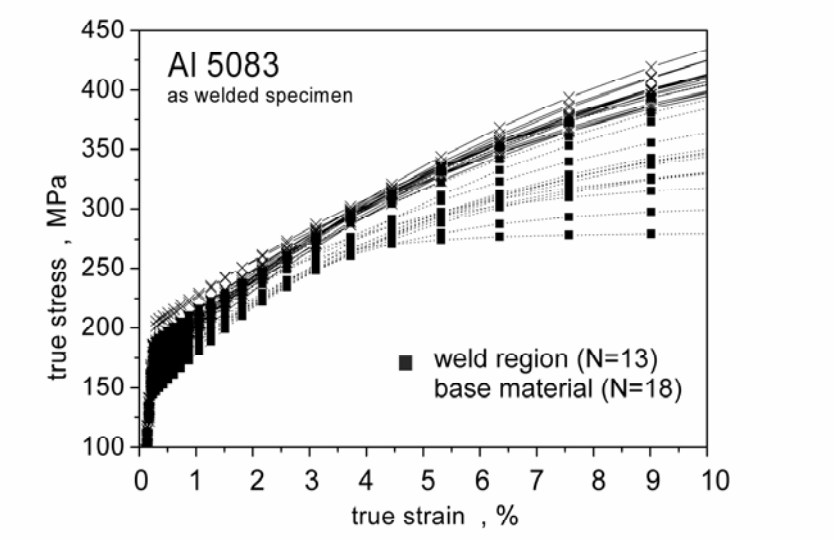

Figure 10a,b:

Local stress-strain curves across the FSW-joint determined via indentation tests applied to an “as-welded” specimen; a) and b) show same curves at different scale.

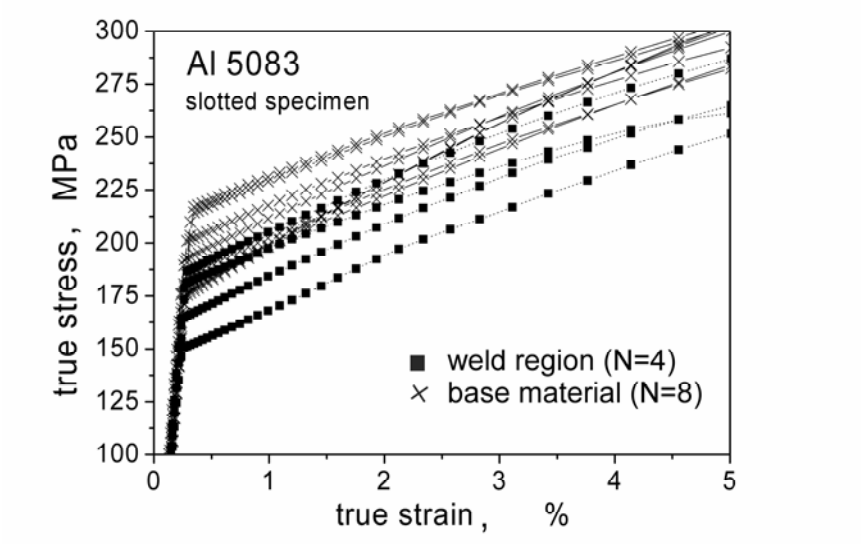

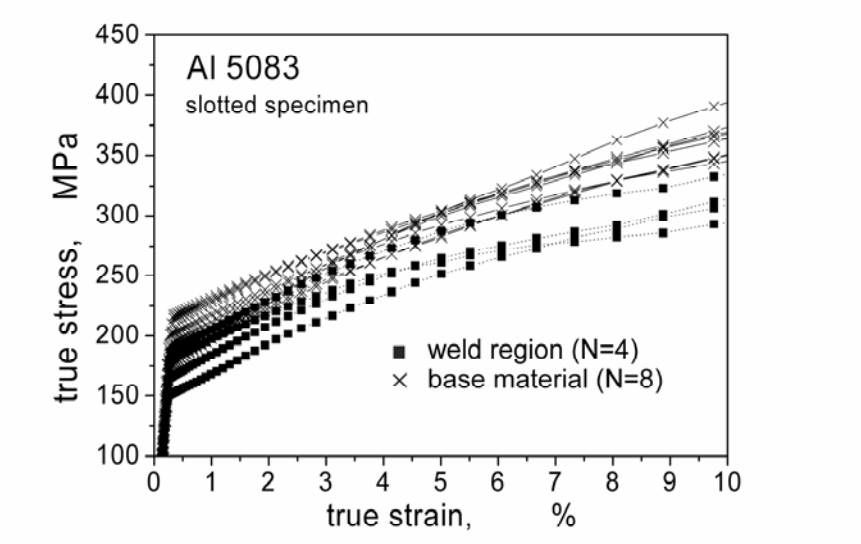

Figure 11a,b:

Local stress-strain curves across the FSW-joint determined via indentation tests applied to a “slotted” specimen; a) and b) show same curves at different scales.

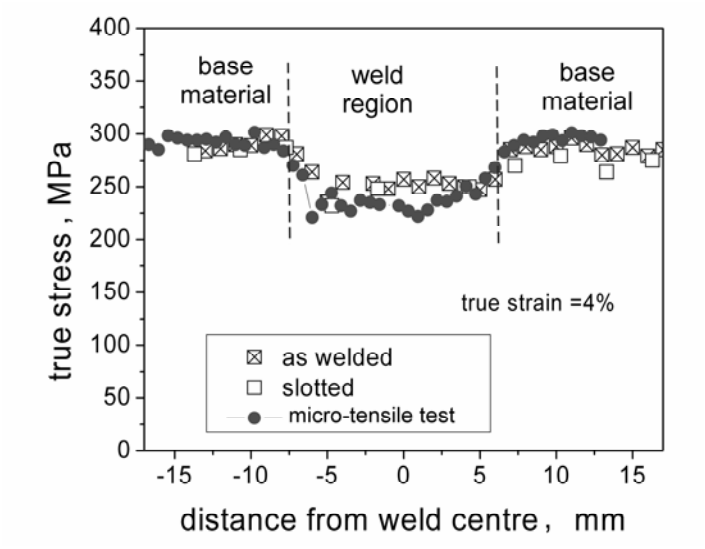

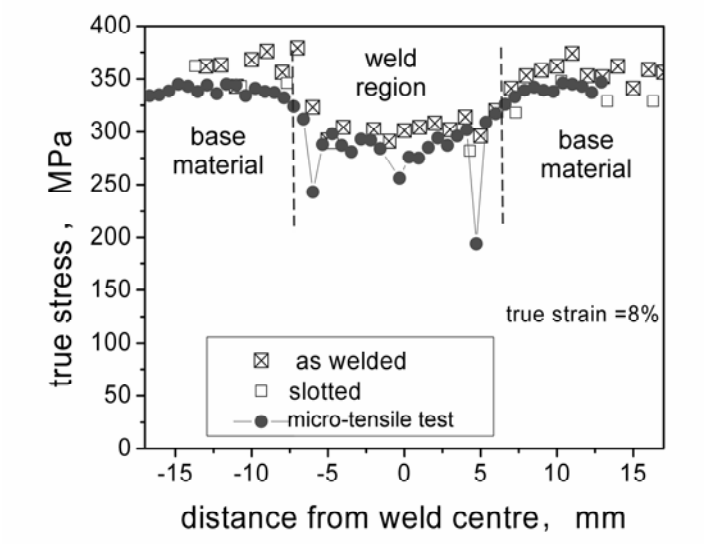

Figure 12a,b:

True-stress values across the weld joint at fixed true-strain values of 4% (a) and 8% (b) as derived by micro-tensile tests and by indentation test on as-welded and slotted indentation specimens.

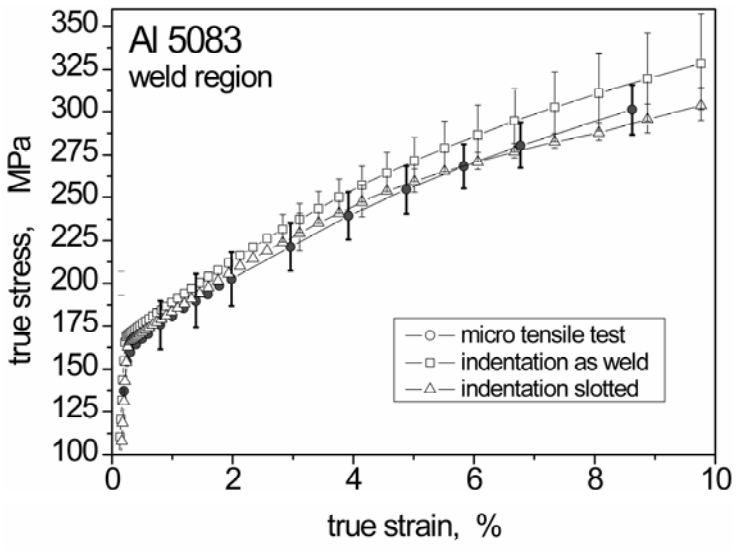

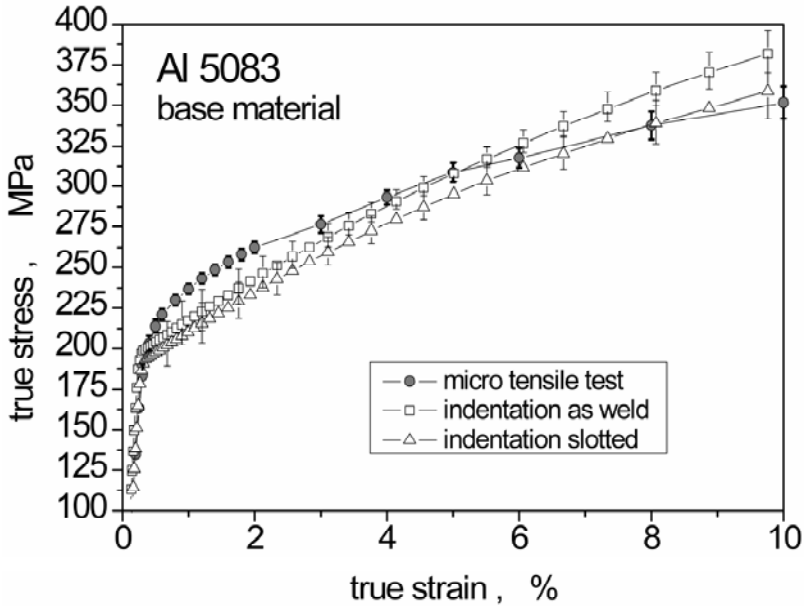

Figure 13a,b:

Average-value true stress-strain curves for a) weld region material and b) base material. The standard deviation is indicated by error-bars.

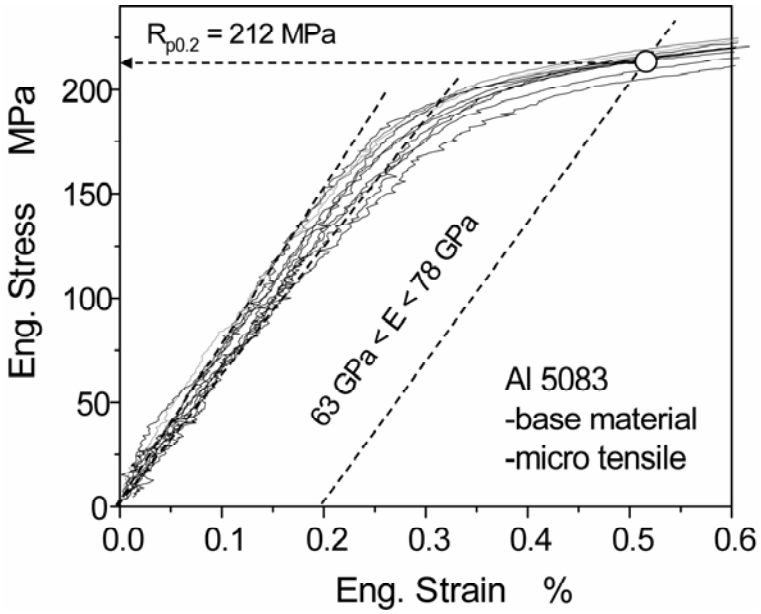

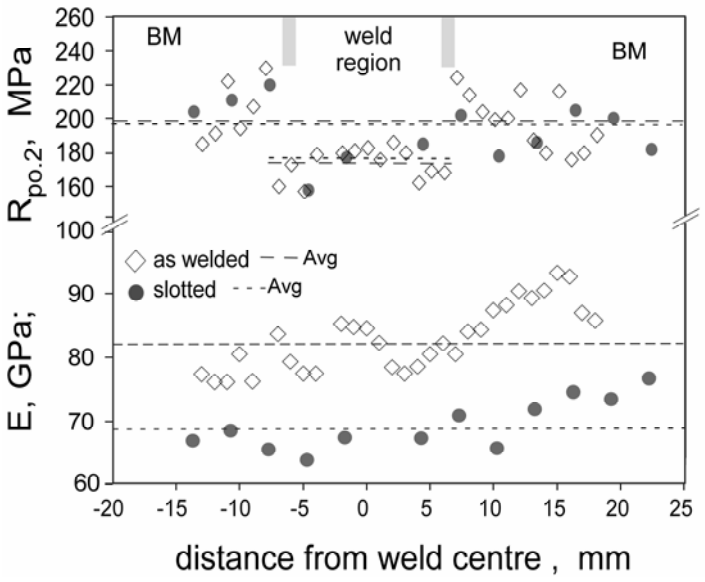

Figure 14a,b:

Comparison of Young's Modulus, E, and 0,2% offset yield strength, $R_{p0.2}$ as derived by micro-tensile tests (a) and by indentation test on as-welded and slotted indentation specimens (b).